Predictive Control with Discrete Space-Vector Modulation of Vienna Rectifier for driving PMSG of Wind Turbine Systems

Lee, June-Seok; Lee, Kyo-Beum; Blaabjerg, Frede

Published in:
IEEE Transactions on Power Electronics

DOI (link to publication from Publisher):
10.1109/TPEL.2019.2905843

Publication date:
2019

Document Version
Accepted author manuscript, peer reviewed version

Citation for published version (APA):
Lee, J-S., Lee, K-B., & Blaabjerg, F. (2019). Predictive Control with Discrete Space-Vector Modulation of Vienna Rectifier for driving PMSG of Wind Turbine Systems. *IEEE Transactions on Power Electronics*, *34*(12), 12368 - 12383. [8675398]. https://doi.org/10.1109/TPEL.2019.2905843

This article has been accepted for publication in a future issue of this journal, but has not been fully edited. Content may change prior to final publication. Citation information: DOI 10.1109/TPEL.2019.2905843, IEEE Transactions on Power Electronics

Predictive Control with Discrete Space-Vector Modulation of Vienna Rectifier for driving PMSG of Wind Turbine Systems

June-Seok Lee, *Member*, *IEEE,* Kyo-Beum Lee, *Senior Member*, *IEEE,* and Frede Blaabjerg, *Fellow*, *IEEE*

***Abstract*—This paper proposes the predictive control with the discrete space-vector modulation (DSVM) for Vienna rectifier connecting to the permanent magnet synchronous generator (PMSG) of the wind turbine system (WTS). Since Vienna rectifier has the special operation principle, Vienna rectifier generates only the feasible 8 voltage vectors, which can be candidate vector for the predictive control, depending on the sign of the input currents. In the proposed predictive control, the feasible voltage vectors are extended from 8 to 19 consisting the 8 original voltage vectors and 11 virtual voltage vectors by using the DSVM for improving the current quality related to the torque ripple, vibration, and noise, and the neutral-point voltage balance with low voltage ripple is guaranteed by using the offset value calculated based on the model of two dc-link capacitors in Vienna rectifier. The scheme for reducing calculation burden is applied in selecting the candidate vector. In addition, the limited operation range for the maximum torque per ampere (MTPA) control of PMSG connected to Vienna rectifier is analyzed. The performance of the proposed predictive control with DSVM for Vienna rectifier with PMSGs is verified in simulation and experiment.**

***Index Terms*—Vienna rectifier, predictive control, wind turbine system, three-level rectifier, permanent magnet synchronous generators.**

I. Introduction

Vienna rectifiers, which are non-generative-boost type, have been extending its applications from the system requiring the power supply [1]-[3] and wind turbine systems (WTS) [4]-[6]. With the application extension of Vienna rectifier, the interest to Vienna rectifier has been increasing in both industry and academia, and the researches on Vienna rectifier have been introduced in lots of field such as topology [7], control method [1]-[5],[8] and so on [9].

In the researches on the control method, two main characteristics of Vienna rectifier have been considered. First one is the special operation condition: the sign of the input voltage of Vienna rectifier should be the same as that of corresponding input current and they should be applied in three phases [1],[10]. Second one is that Vienna rectifier has two dc-link capacitors like thee-level topologies [11]. Owing to it, the control method used in Vienna rectifier should take not only current quality but also the balance of two dc-link capacitors into account [9].

Several representative control methods are introduced as follows: Control method based on the hysteresis was proposed at the beginning of the research [1]. Then, the control methods using the carrier-based pulse-width modulation (CB-PWM) or space-vector modulation (SVM) have been proposed [3],[9]-[10],[12]. In these methods, the proportional-integral (PI) controls, which is already validated in other AC/DC topologies, are used with the transformation principle [9]-[10],[12]. Recently, the model predictive control (MPC) methods for Vienna rectifier are proposed [4]-[6],[13].

The MPC approach has been applied in various power electronics applications. In AC/DC and DC/AC converters especially, the similar MPC approach can be used in various topologies by considering the operation characteristic of its topology. Depending on the topology, however, the control parameters can be different and it should be considered in applying the MPC approach. The simple topology is two-level topology. It has only AC currents as the control parameter in the cost function if the DC-link voltage is fixed (one converter of back-to-back converter used in WTS or motor drive systems).

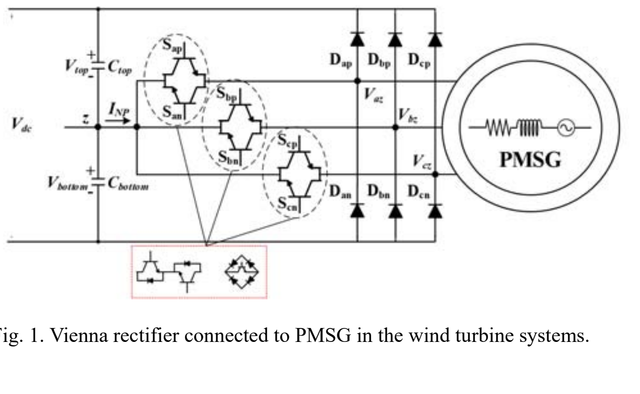

Fig. 1. Vienna rectifier connected to PMSG in the wind turbine systems.

Manuscript received September 21, 2018; revised December 29, 2018; accepted March 3, 2019. This research was supported by a grant(19RTRP-B146008-02) from Railroad Technology Research Program funded by Ministry of Land, Infrastructure and Transport of Korean government.

J-S Lee is with the Propulsion System Research Team, Korea Railroad Research Institute, Uiwang 16105, Seoul, Korea (e-mail: ljs@krri.re.kr).

K.-B. Lee is with the Department of Electrical and Computer Engineering, Ajou University, Suwon 16499, Korea (e-mail: kyl@ajou.ac.kr).

F. Blaabjerg is with the Center of Reliable Power Electronics, Department of Energy Technology, Aalborg University, Aalborg DK-9220, Denmark (e-mail: fbl@et.aau.dk).

Color versions of one or more of the figures in this paper are available online at http://ieeexplore.ieee.org.

Digital Object Identifier -

Therefore, the MPC method used in two-level topology is simple and very intuitive. In the three-level topologies, not only the AC currents but also the neutral-point voltage should be control parameters and they are considered in cost function or vector selection process of MPC [14]-[15]. In addition to the essential control parameters mentioned above, the user requirement such as the number of switching to reduce the switch loss can be added to the control parameter [4].

To improve the performance of MPC in terms of current ripple (or torque ripple), the discrete space vector modulation (DSVM) concept is applied in lots of papers [17]-[20]. A lot of virtual voltage vectors are created by using the DSVM and each virtual voltage vector consists of the several real voltage vectors represented by the switching states. It means that more than two voltage vectors exist in one switching period; therefore, it leads to the current ripple reduction.

The MPC approach has been proposed for Vienna rectifiers [4]-[6],[13]. The conventional FCS-MPC concept is applied to Vienna rectifier in [4] and the feasible 8 vectors on each sector are used. In the process to determine the optimized vector, the neutral-point voltage balance is considered at first, it results in the candidate vectors for applying the FCS-MPC with the cost function consisting current ripples and the number of switching. In [5], the direct torque control for Vienna rectifier considers not only the torque and flux, but also the neutral-point voltage and then the optimized voltage vector generates by the look-up table. In a finite control set-MPC (FCS-MPC) method for Vienna rectifier [6], the neutral-point voltage control has high priority; therefore, the voltage vectors satisfying the defined tolerant value of the neutral-point voltage are selected as candidate vector. Both the neutral-point voltage and current are considered in the cost function of FCS-MPC [13]. The FCS-MPC with DSVM has proposed in [16] and the nineteen voltage vectors become the candidate vector for applying the cost function consisting of the current ripples. Then, the value of neutral-point voltage determines what the optimized voltage vector generates.

This paper is based on the FCS-MPC with DSVM for Vienna rectifier connecting to the permanent magnet synchronous generator (PMSG) of WTS and its configuration is shown in Fig. 1. The proposed FCS-MPC with DSVM, at first, draws the candidate vectors by the proposed voltage vector selection principle; therefore, the calculation burden reduction, which is main disadvantage of FCS-MPC with DSVM, is achieved. Secondly these are used to determine the optimized voltage vector minimizing the cost function consisting the current ripples. Finally, the offset voltage to maintain the neutral-point voltage balance is calculated based on the neutral-point voltage model of Vienna rectifier and is applied to final reference voltages for DSVM because the DSVM enable the offset voltage to be applied. In all process, Vienna rectifier operation requirement is considered as constraints. In addition, the limited operation range for the maximum torque per ampere (MTPA) control of PMSG connected to Vienna rectifier is analyzed.

II. Model of PMSG and Vienna Rectifier

In the proposed FCS-MPC, two models are considered: PMSG model connected to Vienna rectifier and neutral-point voltage model of Vienna rectifier. In this chapter, two models are defined and the operation principle for Vienna rectifier is introduced briefly.

A. PMSG model connected to Vienna rectifier

Vienna rectifier can be considered as voltage source, therefore, the PMSG model used in voltage source inverters [4]-[5],[21] is considered in this paper and it is represented as

$$\begin{aligned} V_{de} &= -R_s i_{de} - L_{ds}\frac{di_{de}}{dt} + \omega_s L_{qs} i_{qe} \\ V_{qe} &= -R_s i_{qe} - L_{qs}\frac{di_{qe}}{dt} - \omega_s L_{ds} i_{de} + \omega_s \lambda_m \end{aligned} , \quad (1)$$

where V_{de}, V_{qe}, i_{de}, i_{qe} are d-axis voltage, q-axis voltage, d-axis current, and q-axis current of Vienna rectifier in the synchronous reference frame, R_s, L_d, and L_q are the stator resistance, d-axis inductance, and q-axis inductance of the PMSG, ω_s is the angular speed of stator, and λ_m is the flux induced by the magnet, respectively.

Equation (1) is transformed to the discrete model with a sampling period T_s. From the discrete model, the d-axis and q-axis currents of Vienna rectifier are predicted as

$$\begin{aligned} & i_{de}[k+1] \\ & = \frac{T_s\left(\omega_s L_{qs} i_{qe}[k] - V_{de}[k]\right)}{L_{ds}} + \left(1 - T_s\frac{R_s}{L_{ds}}\right) i_{de}[k] \\ & i_{qe}[k+1] \\ & = \frac{T_s\left(\omega_s \lambda_m - \omega_s L_{ds} i_{de}[k] - V_{qe}[k]\right)}{L_{qs}} + \left(1 - T_s\frac{R_s}{L_{qs}}\right) i_{qe}[k] \end{aligned} ,(2)$$

where ω_s is variable value depending on time; however, the proposed FCS-MPC assumes that $\omega_s[k] = \omega_s[k+1]$ because the speed is not varied rapidly for T_s in WTS. In case of the surface-mounted PMSG (SPMSG), both L_d and L_q can be substituted to L_s in (1) and (2)

B. Neutral-point voltage model of Vienna rectifier

The neutral-point voltage (V_{NP}) means the difference between the top capacitor voltage (V_{top}) and bottom capacitor voltage (V_{bottom}) of dc-link. V_{NP} is influenced by the neutral-point current (I_{NP}). The neutral-point voltage model of Vienna rectifier is the same as that of three-level topology; therefore, the equation in [9],[11] can be applied for the average I_{NP} calculation during one switching period (T_{sw}), which is T_s in the proposed FCS-MPC, and it is represented as

$$I_{NP} = -(|V_{max}| \cdot I_{max} + |V_{mid}| \cdot I_{mid} + |V_{min}| \cdot I_{min}), \quad (3)$$

where V_{max}, V_{mid}, and V_{min} are maximum, medium, and minimum voltages of V_a, V_b and V_c, respectively, and I_{max}, I_{mid}, and I_{min} are the currents of V_{max}, V_{mid}, and V_{min}, respectively. V_a, V_b and V_c are transformed to V_{qe} and V_{de} of the synchronous reference frame by the coordinates transformation [10],[13].

The discrete equation for neutral-point voltage model of three-level topology in [11] shows the relationship between V_{NP}

This article has been accepted for publication in a future issue of this journal, but has not been fully edited. Content may change prior to final publication. Citation information: DOI 10.1109/TPEL.2019.2905843, IEEE Transactions on Power Electronics

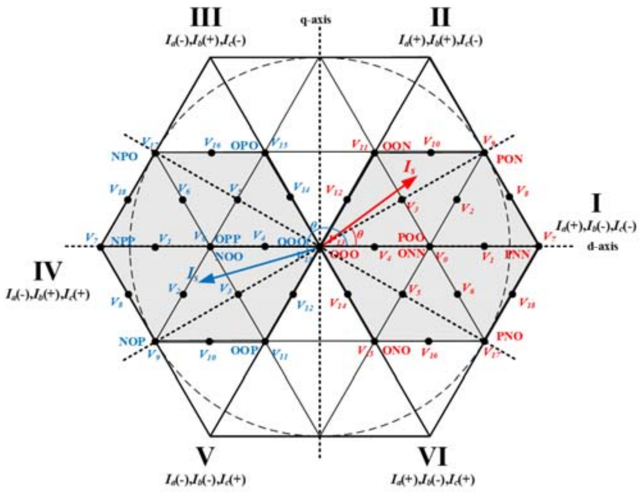

Fig. 2. The DSVM based voltage vector diagram used in the proposed FCS-MPC.

and I_{NP} and it is represented as

$$\begin{aligned} V_{NP}[k+1] &= V_{top}[k+1] - V_{bottom}[k+1] \\ &= V_{NP}[k] + \frac{1}{C} I_{NP}[k+1] T_s \\ &= V_{NP}[k] \\ &\quad + \frac{2T_s}{V_{dc}C}\Big(\left|V_{max}(k+1)\right| \cdot I_{\max}(k+1) \\ &\quad + \left|V_{mid}(k+1)\right| \cdot I_{mid}(k+1) \\ &\quad + \left|V_{\min}(k+1)\right| \cdot I_{\min}(k+1) \Big) \end{aligned} , \quad (4)$$

where C is the capacitance of dc-link.

C. Vienna rectifier operation

Vienna rectifier using the bidirectional switch of Fig. 1 is considered in this paper. There are three switching states (P, O, and N). The P-switching state indicates S_{xp}(ON) and S_{xn}(OFF) and N-switching state means S_{xp}(OFF) and S_{xn}(ON). The O-switching state occurs by S_{xp}(ON) and S_{xn}(ON). Each leg has the switching state of P, O, and N, and the combination of three legs are expressed as the voltage vectors shown in Fig. 2.

Vienna rectifier has the requirement for regulating the sinusoidal currents. The polarity of a leg's voltage of Vienna rectifier should be the same as the polarity of a corresponding leg's current [1],[10]. Therefore, depending on polarity of the three currents, the voltage vectors for applying to the FCS-MPC should be limited as shown in Fig. 2. Therefore, the first step for the proposed FCS-MPC is to fine out Sector containing the current vector (I_s). Sector can be determined by using the three leg currents and it is summarized in Table I.

III. The Proposed FCS-MPC with DSVM for Vienna Rectifier

All steps of the proposed FCS-MPC with DSVM are shown in Fig. 3. There are four steps: Step I. Voltage vector selection, Step II. Current control, Step III. Neutral-point voltage control, and Step IV. Reference voltage decision. The proposed FCS-MPC with DSVM for Vienna rectifier focuses on two control targets: the input current and neutral-point voltage of Vienna rectifier. In this chapter, each step is explained in order.

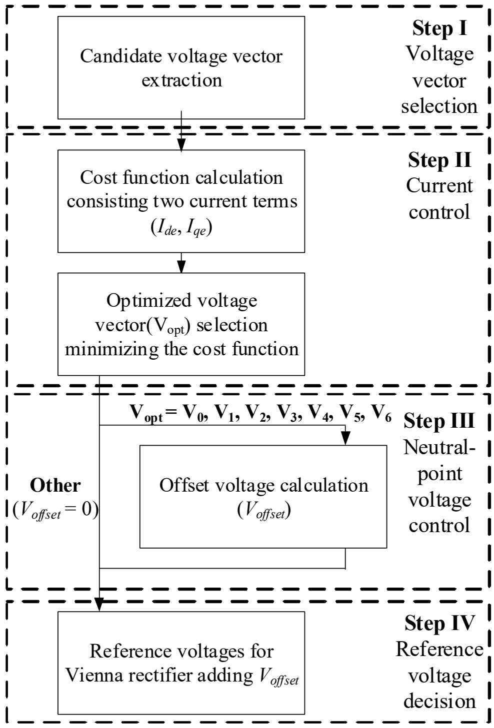

Fig. 3. Flowchart of the proposed FCS-MPC with DSVM.

TABLE I
Sign of Input Currents Depending on Sector

Sector	Current	Sector	Current
I	$i_a(+)$, $i_b(-)$, $i_c(-)$	IV	$i_a(-)$, $i_b(+)$, $i_c(+)$
II	$i_a(+)$, $i_b(+)$, $i_c(-)$	V	$i_a(-)$, $i_b(-)$, $i_c(+)$
III	$i_a(-)$, $i_b(+)$, $i_c(-)$	VI	$i_a(+)$, $i_b(-)$, $i_c(+)$

A. Step I: Voltage vector selection

The conventional MPC just has the 8 voltage vectors per each Sector in Vienna rectifier [4][13]. However, there are totally 19 voltage vectors per each Sector in Fig. 2. It is because the DSVM allows the voltage vectors to be divided. It means that the current quality can be improved. Nevertheless, the DSVM aggravates the computation burden in applying the FCS-MPC owing to increasing the number of candidate vectors. Therefore, this paper suggests the method for extracting the effective candidate voltage to reduce the computation burden.

The voltage vector selection method is established to achieve the minimization of the current ripple in the current control. To reduce the current ripple, the voltage vectors closed to the desired voltage vector (V_{ref}) generating the desired current (I_s) should be selected. In step of the voltage vector section, the magnitude of V_{ref} is used and $|V_{ref}|$ is calculated from (1) as

$$\left|V_{ref}\right| = \sqrt{\begin{aligned} &\left(-R_s i_{de,ref} - L_{ds}\frac{di_{de,ref}}{dt} + \omega_s L_{qs} i_{qe,ref}\right)^2 \\ &+\left(-R_s i_{qe,ref} - L_{qs}\frac{di_{qe,ref}}{dt} - \omega_s L_{ds} i_{de,ref} + \omega_s \lambda_m\right)^2 \end{aligned}} , \quad (5)$$

This article has been accepted for publication in a future issue of this journal, but has not been fully edited. Content may change prior to final publication. Citation information: DOI 10.1109/TPEL.2019.2905843, IEEE Transactions on Power Electronics

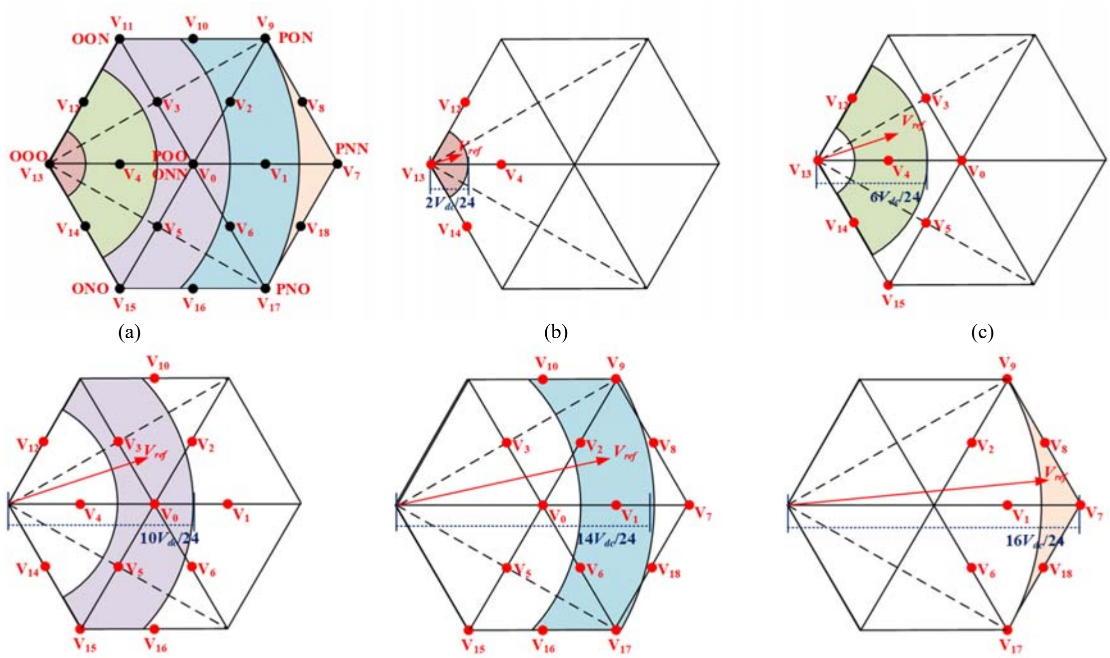

Fig. 4. Voltage vector selection depending on $|V_{ref}|$. (a) All levels. (b) Level 0. (c) Level 1. (d) Level 2. (e) Level 3. (f) Level 4.

TABLE II
VOLTAGE VECTOR SELECTION DEPENDING ON $|V_{REF}|$

Level	$\|V_{ref}\|$	Candidate vectors	Number of candidate vectors
0	$0 < \|V_{ref}\| \le 2V_{dc}/24$	$V_4, V_{12}, V_{13}, V_{14}$	4
1	$2V_{dc}/24 < \|V_{ref}\| \le 6V_{dc}/24$	$V_0, V_3, V_4, V_5, V_{12}, V_{13}, V_{14}, V_{15}$	8
2	$6V_{dc}/24 < \|V_{ref}\| \le 10V_{dc}/24$	$V_0, V_1, V_2, V_3, V_4, V_5, V_6, V_{10}, V_{12}, V_{14}, V_{15}, V_{16}$	12
3	$10V_{dc}/24 < \|V_{ref}\| \le 14V_{dc}/24$	$V_0, V_1, V_2, V_3, V_5, V_6, V_7, V_8, V_9, V_{10}, V_{15}, V_{16}, V_{17}, V_{18}$	14
4	$14V_{dc}/24 < \|V_{ref}\| \le 16V_{dc}/24$	$V_1, V_2, V_6, V_7, V_8, V_9, V_{17}, V_{18}$	8

where $i_{de,ref}$ is d-axis reference current indicating the flux of PMSG and $i_{qe,ref}$ is q-axis reference current indicating the torque of PMSG. The dominant component of $|V_{ref}|$ is $\omega_s\lambda_m$ which is proportional to the speed of the PMSG and the deferential terms in (5) exists only during the transient state where the one or two of $i_{de,ref}$ and $i_{qe,ref}$ are changed.

Based on the voltage vector diagram of Fig. 2, $|V_{ref}|$ belongs to one of five levels as shown in Fig. 4(a). Depending on $|V_{ref}|$, the voltage vectors are extracted as the candidate vector. As the example, the V_0, V_3, V_4, V_5, V_{12}, V_{13}, V_{14}, and V_{15} are selected as the candidate vector for applying the cost function where $|V_{ref}|$ is between $2V_{dc}/24$ and $6V_{dc}/24$, and it is Level 1 as shown in Fig. 4(c). All cases of Fig. 4(b) – (f) are summarized in Table II.

Two voltage vectors V_{11} and V_{15} are placed on other Sector; therefore, it is not necessary to consider two voltage vectors. However, V_{15} is contained in Fig. 4(c) – (e). In the normal operation of converter with the PMSG, the converter voltage and the counter electromotive force (V_{EMF}) of PMSG have the phase difference to generate the current flow [22] and the current angle is matched at (unity power factor) or move with respect to the angle of V_{EMF} (legging current or leading current condition). Therefore, V_{11} and V_{15} can be used because of the phase difference between the current and V_{EMF}. Since the rectifier has only the leading current with respect to V_{EMF}; however, only V_{15} is considered in this paper.

B. Step II: Current Control (FCS-MPC)

Step 2 is the current control. The FCS-MPC is used as the current controller to improve current quality extremely. The neutral-point voltage can be controlled by the injection of offset voltage because of the DSVM used in this paper. In the current control, the d-axis current (i_{de}) and q-axis current (i_{qe}) of Vienna rectifier in the synchronous reference frame are used as the control variable. i_{de}[k+1] and i_{qe}[k+1] depending on the voltage vector (V_i) are estimated from (2) and they are expressed as

$$(i_{de}[k+1][V_i], i_{qe}[k+1][V_i]), \quad i = \text{(Table II)}. \tag{6}$$

Although the various constructions of the cost function (CF) are showing in lots of papers [4]-[6],[14]-[15], only i_{de}[k+1][V_i] and i_{qe}[k+1][V_i] are applied to calculate CF. Therefore, CF is expressed as

$$CF = (i_{de,ref} - i_{de}[k+1][V_i])^2 + (i_{qe,ref} - i_{qe}[k+1][V_i])^2, \quad i = \text{(Table II)}. \tag{7}$$

Then V_i minimizing (7) is selected as the optimized voltage vector (V_{opt}) and it is expressed as

$$V_{opt} \leftarrow \min_{i=\text{Table II}} CF[V_i]. \tag{8}$$

C. Step III: Neutral-Point Voltage Control

The proposed control is based on the DSVM. It means that

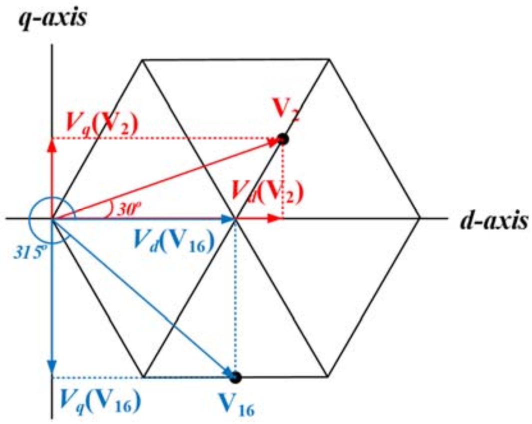

Fig. 5. The calculation of d-axis value (V_d) and q-axis value (V_d) of V_i.

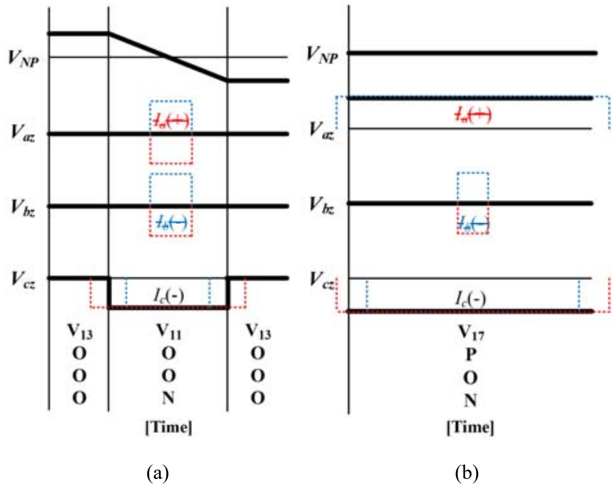

Fig. 6. V_{NP} and switching sequence of voltage vectors of Group I in Sector I. (a) V_{12}. (b) V_{17}.

the switching state cannot be fixed in one switching period. Therefore, the offset voltage (V_{offset}) can be used to change three reference voltages (V_a, V_b, V_c). Adding V_{offset} to V_a, V_b, and V_c influences on the variation of V_{NP} [9]-[10]. The adjustable V_{offset} keeps V_{NP} to zero with the maintenance of the input current quality.

To apply V_{offset}, V_i should be represented to V_a, V_b, and V_c. In first, d-axis value (V_d) and q- axis value (V_q) of V_i are calculated from the space vector diagram of Fig. 5. In this transformation, the degree (θ_{dq}) between V_i and the d-axis which is expressed with the stator angle (θ_s) of the PMSG, and the magnitude ($|V_i|$) of V_i are needed to calculate $V_d[V_i]$ and $V_q[V_i]$ and they are expressed as

$$\begin{aligned} V_d[\mathrm{V}_i] &= |\mathrm{V}_i|\cos\theta_{dq} \\ V_q[\mathrm{V}_i] &= |\mathrm{V}_i|\sin\theta_{dq} \end{aligned} \quad ,\theta_{dq} = \theta_s + \frac{\pi}{2}. \tag{9}$$

Then, the result of (9) is represented to V_a, V_b, and V_c thought the abc-dq transformation and they are expressed as

$$\begin{aligned} V_a[\mathrm{V}_i] &= V_d[\mathrm{V}_i] \\ V_b[\mathrm{V}_i] &= -\frac{1}{2}V_d[\mathrm{V}_i] + \frac{\sqrt{3}}{2}V_q[\mathrm{V}_i] \\ V_c[\mathrm{V}_i] &= -\frac{1}{2}V_d[\mathrm{V}_i] - \frac{\sqrt{3}}{2}V_q[\mathrm{V}_i] \end{aligned} . \tag{10}$$

All V_i cannot reflect V_{offset}. To define the feasible V_i permitting that V_{offset} can be added, the nineteen V_i are classified to two groups: Group I is [V_8, …, V_{18}] and Group II is [V_0, …, V_6]. Group I means that it is not possible to add V_{offset} to their voltage vectors. Fig. 6 shows the switching sequence of the representative voltage vectors in Group I when current vector is located in Sector I. V_{12} is configured by the two voltage vectors (V_{11} and V_{13}) near itself and the V_{NP} is changed by only V_{11}. This configuration is shown in V_8, V_{10}, V_{14}, V_{16}, and V_{18}, similarly. V_{NP} is effected by V_9, V_{11}, V_{15}, and V_{17} who are defined as the small vector or medium vector. In addition, adding V_{offset} violates the rule of Vienna rectifier operation. In the case of the positive V_{offset}, the switching sequence is changed as blue dot-line of Fig. 6(a) and the polarity (+) of the changed V_{bz} is not the same as I_b(-). The negative V_{offset} leads to the red dot-line of Fig. 6(a) where the violated situation in a-leg. Consequently, V_{NP} is not controllable if the voltage vector of the Group I is determined as the optimized voltage vector. Fig. 6(b) shows the case of V_{17} consisting of only itself like V_9, V_{11}, V_{13}, V_{15}, and V_{17}. Similar to V_{12}, the violated situation occurs when V_{offset} is added.

Group II consists of the voltage vectors what can change V_{NP} by adding the V_{offset}. The characteristic is similar to that of three-level topologies [11], [14]. Since Vienna rectifier has the operation constrain, the completed freedom in applying V_{offset} is not assigned in the neutral-point voltage control.

The range of V_{offset} is determined from the switching sequence analysis. The switching sequence of V_4 in Sector I has the two voltage vectors (V_0, V_{13}) but there are three switching states ([OOO], [POO], [ONN]) as shown in Fig. 7(a). [POO] and [ONN] have the same equivalent three-leg output voltage but influence on V_{NP} in the opposite side. Depending on how to add V_{offset} to V_4, although the three-leg output voltages are fixed as desired value, V_{NP} can be changed. Fig. 7(b) shows the waveform changed by the positive and negative V_{offset}s. When the positive V_{offset} raises up V_{NP} as the line of Fig. 7(b) and it increases the ON-time (T_{POO}) of [POO] decreases the ON-time (T_{ONN}) of [ONN]. The negative V_{offset} leads to the decrement of V_{NP}. V_{offset} can be added until the ON-time of [POO] or [ONN] becomes zero. Therefore, the range of V_{offset} for V_4 is related to T_{ONN} and T_{POO}. The T_{ONN} and T_{POO} in V_4 are the same as $|T_{min}|$ and $|T_{max}|$ respectively. They are defined by using three-leg ON-times ($|T_a|$, $|T_b|$ and $|T_c|$): T_{max} and T_{min} are the maximum and minimum values of T_a, T_b and T_c calculated from V_a, V_b, V_c, respectively. The relationship between T_a, T_b, T_c and V_a, V_b, V_c is represented as

$$T_x = \frac{2V_x}{V_{dc}}T_s \quad x = a, b, c, \tag{11}$$

where T_s is a switching period. If T_x is negative, the negative voltage ($-V_{dc}/2$) is generated and the ON-time is $|T_x|$ as shown in V_{bz} and V_{cz} of Fig. 7. Consequently, the range of V_{offset} for V_4 is represented as

$$\frac{V_{dc}T_{min}}{2T_s} < V_{offset} < \frac{V_{dc}T_{max}}{2T_s}, \tag{12}$$

Fig. 8 shows that V_2 is selected as V_{opt}. V_2 consists of

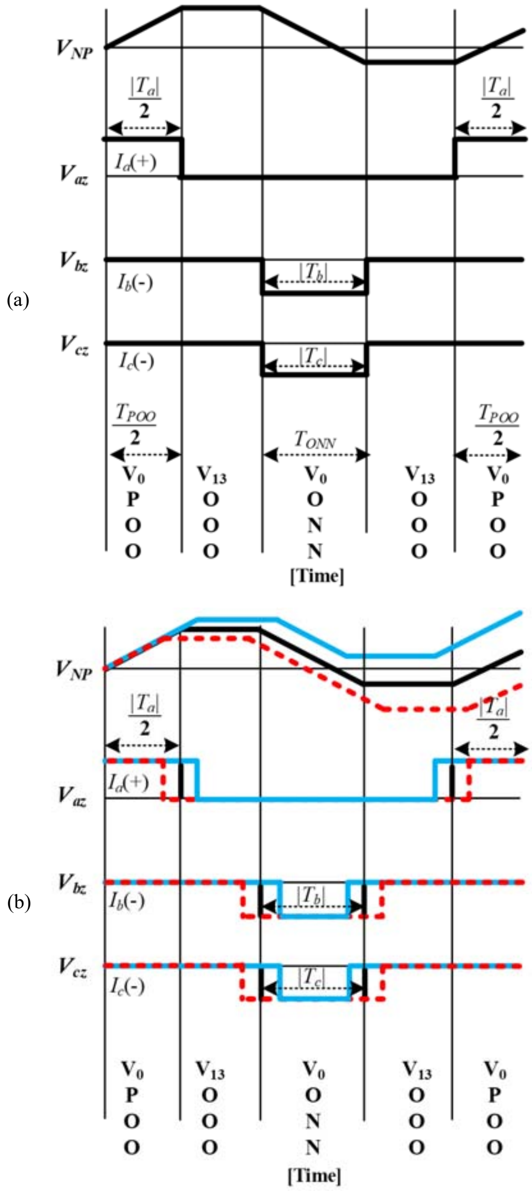

Fig. 7. V_{NP} and switching sequence of V_4 in Sector I. (a) Zero V_{offset}. (b) Positive V_{offset} (line) and negative V_{offset} (dotted-line).

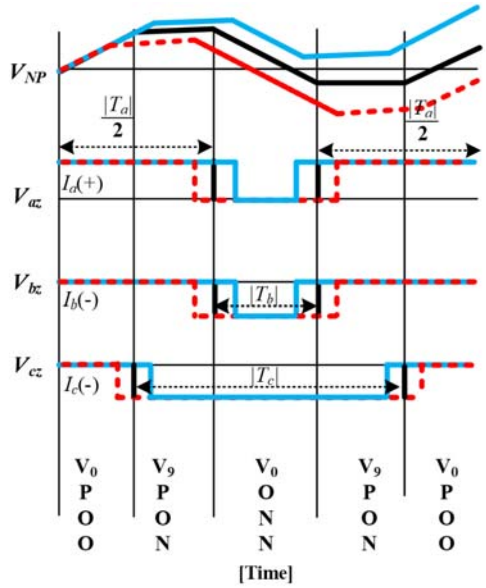

Fig. 8. V_{NP} and switching sequence of V_2 in Sector I: Positive V_{offset} (line) and negative V_{offset} (dotted-line).

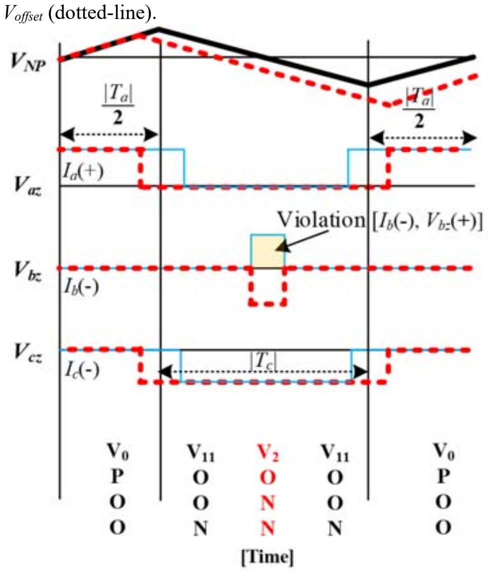

Fig. 9. V_{NP} and switching sequence of V_3 in Sector I: Positive V_{offset} (line, infeasible case) and negative V_{offset} (dotted-line).

three-switching states: POO, PON, and ONN. The analysis background for adding V_{offset} to V_2 is the same as the case of V_4 mentioned above. However, since making the T_{POO} and T_{ONN} to zero is determined by OFF-time ([T_s-T_a], [T_s-T_b], [T_s-T_c]), the range of V_{offset} is expressed as

$$-\frac{V_{dc}(T_s+T_{min})}{2T_s} < V_{offset} < \frac{V_{dc}(T_s-T_{max})}{2T_s}, \tag{13}$$

equation (13) can be applied when V_0, V_1, V_2, or V_6 is V_{opt}.

When the V_3 or V_5 is determined as V_{opt}, the bi-directional V_{NP} variation is possible. In case of V_3, there are two switching states: POO and OON. Among them, T_{POO} can be only decreased by the negative V_{offset}. If the positive V_{offset} is added, the range where Vienna rectifier operation rule is violated appears as shown in Fig. 9. Therefore, the range of V_{offset} for V_3 and V_5 in Sector I, III, V is represented as

$$-\frac{V_{dc}(T_s+T_{min})}{2T_s} < V_{offset} < 0\,. \tag{14}$$

In cases of V_3 and V_5, the bi-directional V_{NP} variation is determined by Sector. If Sector is odd as shown in Fig. 9, V_{NP} only decreases by adding the negative V_{offset}. On the other hand, the even Sector permits V_{NP} to be increased only when V_3 or V_5 is selected as V_{opt} by adding the positive V_{offset} Therefore, in even Sector II, IV, VI, the range of V_{offset} is changed as

$$0 < V_{offset} < \frac{V_{dc}(T_s-T_{max})}{2}, \tag{15}$$

the summarized principle for the range of V_{offset} is shown in Table III.

In order to calculate the adjustable V_{offset} to make V_{NP} zero, the neutral-point voltage model of (4) is used. The equation with the V_{offset} making $V_{NP}[k+1]$ zero is represented as

This article has been accepted for publication in a future issue of this journal, but has not been fully edited. Content may change prior to final publication. Citation information: DOI 10.1109/TPEL.2019.2905843, IEEE Transactions on Power Electronics

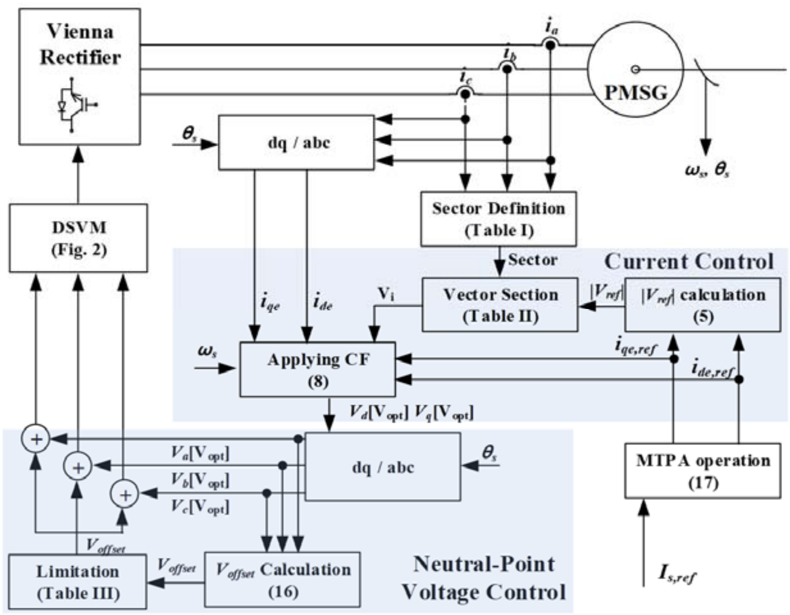

Fig. 10. The block diagram of the proposed predictive control with the discrete space-vector modulation (DSVM).

TABLE III
THE RANGE OF V_{OFFSET} DEPENDING ON VOLTAGE VECTOR

Voltage vector	The range of V_{offset}
V_4	$V_{min} < V_{offset} < V_{max}$
V_3, V_5	Odd Sector: $-V_{dc}/2 - V_{min} < V_{offset} < 0$ Even Sector: $0 < V_{offset} < V_{dc}/2 - V_{max}$
V_0, V_1, V_2, V_6	$-V_{dc}/2 - V_{min} < V_{offset} < V_{dc}/2 - V_{max}$

$$V_{NP}[k] = \frac{2T_s}{V_{dc}C}\Big(\left|V_{max}(k+1)+V_{offset}\right|\cdot I_{\max}(k+1) + \left|V_{mid}(k+1)+V_{offset}\right|\cdot I_{mid}(k+1) + \left|V_{\min}(k+1)+V_{offset}\right|\cdot I_{\min}(k+1)\Big) = 0 \quad (16)$$

D. Step IV: Reference Voltage Decision

The reference voltages for Vienna rectifier are determined finally adding V_{offset} calculated from (16) to V_a, V_b, and V_c. Fig. 10 shows the block diagram of the proposed predictive control FCS-MPC with DSVM.

IV. FEASIBLE MTPA RANGE OF PMSG DRIVEN BY VIENNA RECTIFIER

The PMSG can be divided into two types: the surface mounted PMSG (SPMSG) and interior PMSG (IPMSG) depending on the shape of the magnet inserted to rotor [23]. To achieve MTPA in SPMSM, the d-axis current meaning the flux is controlled to zero and only q-axis current meaning the torque has the desired value. However, the MTPA control of the IPMSM requires the injection of d-axis current which is not zero. Lots of studies [23]-[24] had been researched to determine the value of the d-axis current for the MTPA control and it is expressed as

$$i_{de,ref} = -I_{s,ref}\sin\theta_\beta$$
$$i_{qe,ref} = I_{s,ref}\cos\theta_\beta$$
$$\theta_\beta = \sin^{-1}\left(\frac{-\lambda_m+\sqrt{\lambda_m^2+8(L_q-L_d)^2 I_{s,ref}^2}}{4(L_q-L_d)I_{s,ref}}\right), \quad (17)$$

where $I_{s,ref}$ is the magnitude of the current.

The θ_β of (16) is the angle for calculating the power factor. It means that the IMPSG is driven at different power factor by the MTPA control. Since Vienna rectifier operates at the limited power factor which is from 0.866 to 1, the possibility of MTPA control for the IPMSG should be considered. As represented in (16), the condition of MTPA control depends on the parameters of the IPMSG. In Vienna rectifier, the limited power factor which is 0.866 means that θ_β is 30°; therefore, by using (16) the limited condition of the MTPA control is expressed as

$$\sin(30^o) < \frac{-A+\sqrt{A^2+8B^2I_s^2}}{4BI_s}, \quad (18)$$

where A is λ_m and B is $L_q - L_d$. The roots of (A, B) satisfying (18) shows the specifications of IPMSG for applying the MTPA control in Vienna rectifier.

Equation (18) does not reflect the angle drop (θ_z) caused by the impedance of IPMSG stator. If the stator current is large, it cannot be ignored. In general, the power factor is defined by the θ_β between the current and V_{EMF}. However, the power factor (pf_V) to explain the operation range of Vienna rectifier is defined by the angle difference (θ_v) between the current and reference voltage (V_{ref}). Fig. 11 shows the key waveforms in generating the current between IPMSG and Vienna rectifier. In Fig. 11, the feasible range of θ_v is located with V_{ref} as the center equally and the applicable θ_β is reduced owing to θ_z caused by the impedance of IPMSG stator. Therefore, θ_β is limited as

$$\theta_\beta < 30^o - \theta_z, \quad (19)$$

The limited θ_β of (19) should be taken into account in (18)

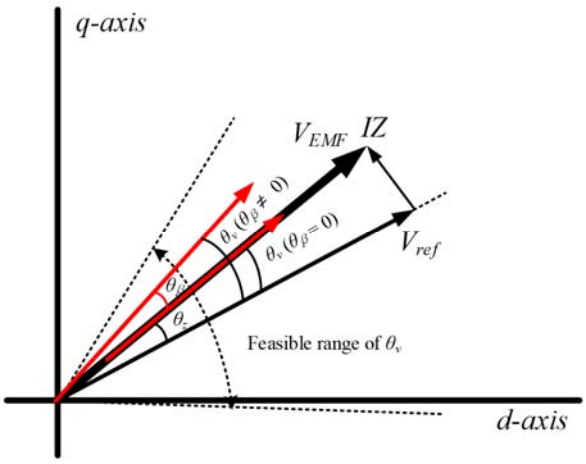

Fig. 11. Current and voltage waveforms of Vienna rectifier and IPMSG

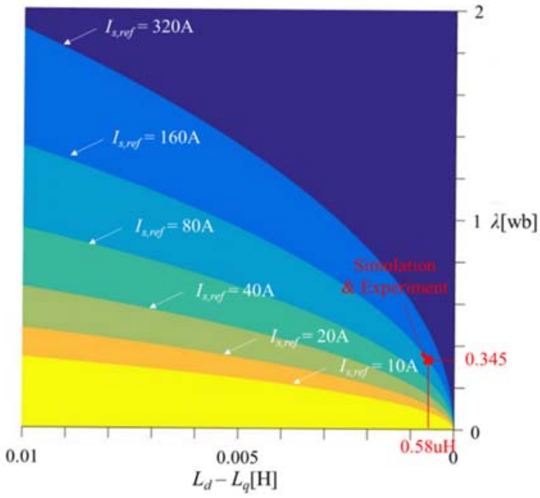

Fig. 12. The applicable parameters for MTPA control of IPMSG driven by Vienna rectifier depending on $I_{s,ref}$.

TABLE IV
IPMSG PARAMETERS

Number of pole	6
Rated voltage (line-to-line)	191 V_{rms}
Rated speed	1450 r/min
R_s	0.099 Ω
$L_{q,real}/L_{d,real}$	4.65 mH /4.07 mH

then, (18) is represented as

$$\sin(30^o - \theta_z) < \frac{-A + \sqrt{A^2 + 8B^2 I_s^2}}{4BI_s}$$
$$\theta_z = \left| \tan^{-1}\left(\frac{-R_s i_{de,ref} + \omega_s L_{qs} i_{qe,ref}}{-R_s i_{qe,ref} - \omega_s L_{ds} i_{de,ref} + \omega_s \lambda_m} \right) \right|, \quad (20)$$

where θ_z is calculated from (1). In Fig. 12, the range above each curve indicates the IPMSG parameters (L_d-L_q, λ) enabling the MTPA control in Vienna rectifier depending on I_s.

V. SIMULATION RESULTS

The simulation results to identify the performance of the FCS-MPC with DSVM are shown in this chapter. The simulation circuit is the same as Fig. 1 and the PMSG parameters of Table IV is used. The dc-link voltage is 300V, the dc-link capacitor are 1100 uF, and the sampling period (T_s) is 200 us. The $i_{de,ref}$ and $i_{qe,ref}$ are calculated by (17).

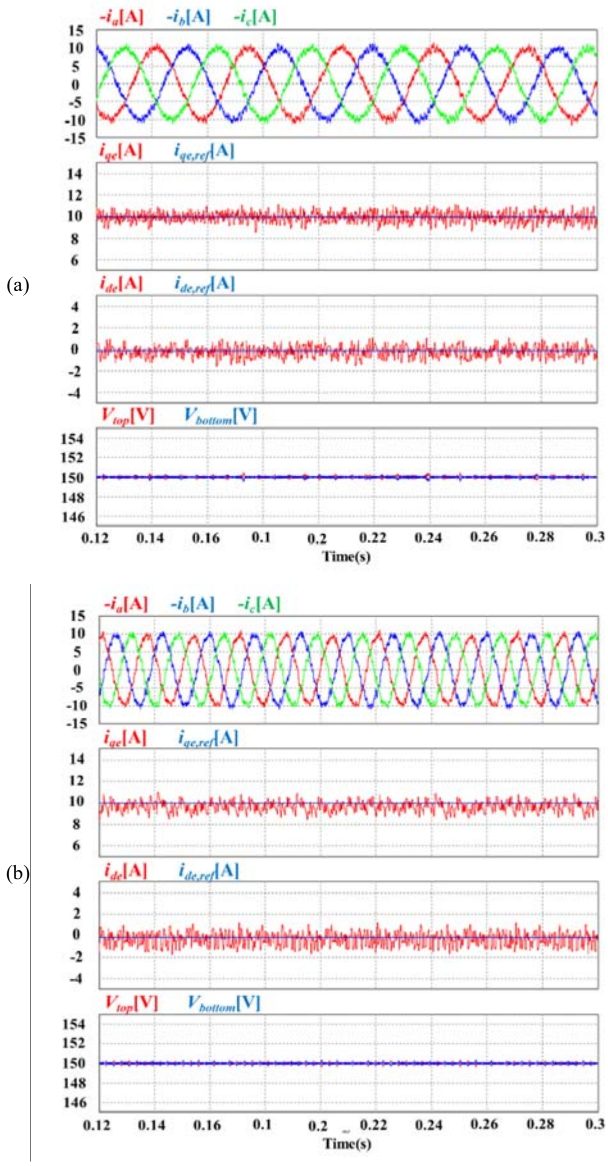

Fig. 13. Simulation results of the FCS-MPC with DSVM depending on the speed: $I_{s,ref}$ (10A). (a) Speed (600 r/m). (b) Speed (1200 r/m).

Fig. 13 shows the simulation results of the FCS-MPC with DSVM depending on the speed. Since $I_{s,ref}$ is set as 10 A, the $i_{qe,ref}$ and $i_{de,ref}$ are calculated as about 9.99 A and -0.17 A through the MTPA control. It is identified that the three leg currents are balanced and controlled as the desired value. Two dc-link voltages (V_{top} and V_{bottom}) have the same value which means that the neutral-point voltage balance is achieved.

Fig. 14 and Fig. 15 show key waveforms of the FCS-MPC with DSVM. When the speed is 600 r/m, $|V_{ref}|$ is located between $2V_{dc}/24$ and $6V_{dc}/24$ as shown in Fig. 14(a). Therefore, only 8 voltage vectors (V_0, V_3, V_4, V_5, V_{12}, V_{13}, V_{14}, V_{15}) becomes the candidate vector. In addition, it can be identified that the one vector of the 8 voltage vectors is determined as V_{opt} through the third waveform which shows the voltage vector number selected in Fig. 14(a). In Fig. 14(b), V_{offset} is calculated

This article has been accepted for publication in a future issue of this journal, but has not been fully edited. Content may change prior to final publication. Citation information: DOI 10.1109/TPEL.2019.2905843, IEEE Transactions on Power Electronics

(a)

(b)

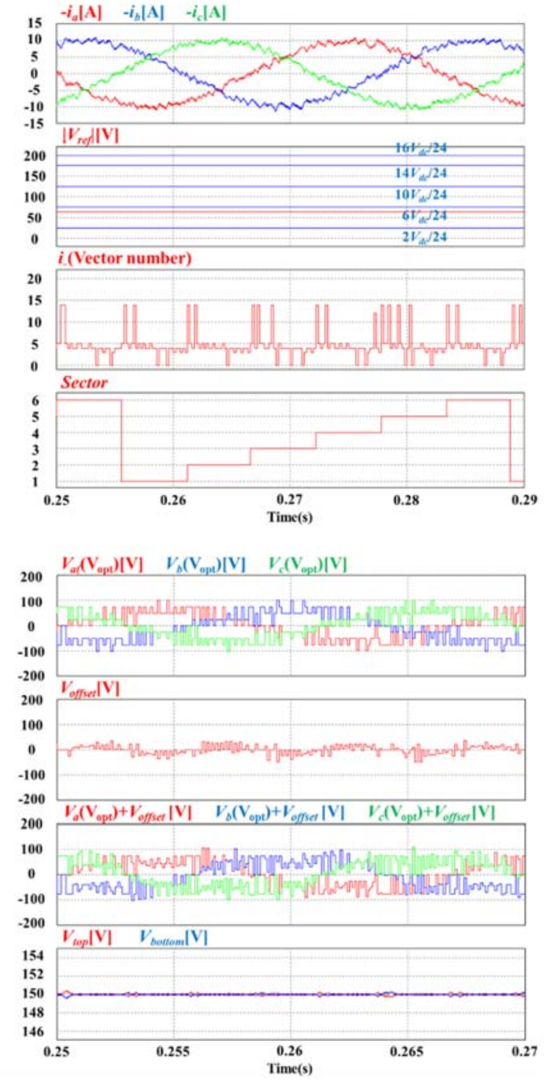

Fig. 14. Key waveforms of the FCS-MPC with DSVM when the speed is 600 r/m: $I_{s,ref}$ (10A). (a) Related to the neutral-point voltage control. (b) Related to the current control.

(a)

(b)

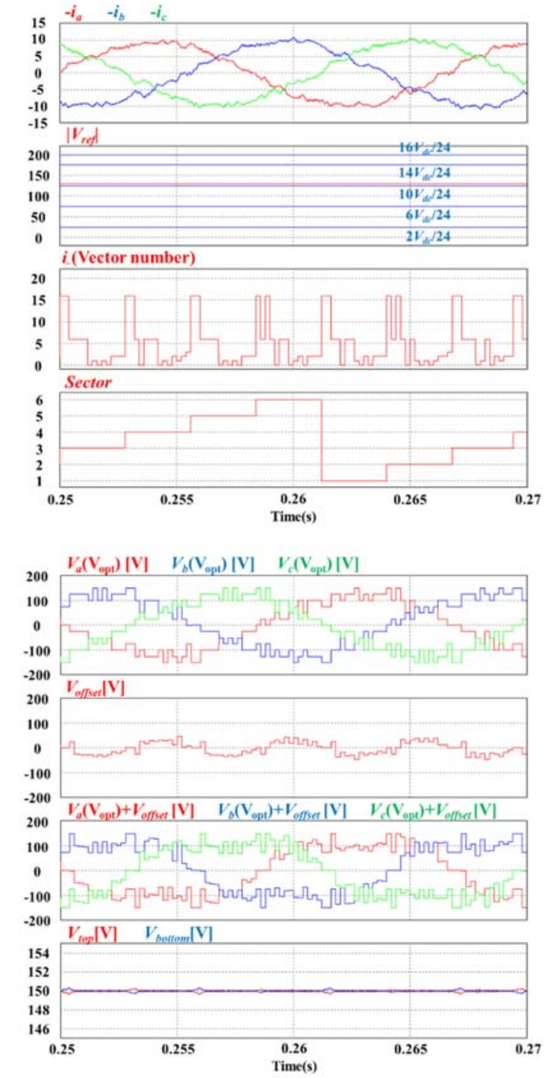

Fig. 15. Key waveforms of the FCS-MPC with DSVM when the speed is 1200 r/m: $I_{s,ref}$ (10A). (a) Related to the neutral-point voltage control. (b) Related to the current control.

and influences on the two dc-link voltages (V_{top}, V_{bottom}). Although the calculated V_{offset} is added to V_x[V_{opt}], the region where the voltage difference between V_{top} and V_{bottom} is not almost zero appears periodically as shown in last one of Fig. 14(b). It is because that only several voltage vectors can accept V_{offset}; furthermore, V_{offset} is limited to value defined in Table III depending on the selected voltage vector. The evidences at 1200 r/m which are the same as Fig. 14 are shown in Fig. 15.

Fig. 16 shows the neutral-point voltage control ability of the FCS-MPC with DSVM. The neutral-point voltage unbalance is generated by connecting the resistor to the top side capacitor (C_{bottom}) in parallel. For the neutral-point voltage control, V_{offset} calculated from (16) is applied after 0.25s. It is shown that the neutral-point voltage becomes almost zero by V_{offset} in Fig. 16.

In Fig. 17, the θ_z and θ_β are changed as $I_{s,ref}$ incensement. In case of $I_{s,ref}$ (10A), the θ_z and θ_β are 7.8˚ and 1.0˚ respectively and the summation of them does not exceed 30˚ which is the operation limitation angle for Vienna Rectifier. After $I_{s,ref}$ is changed to 20 A, the summation is under 30˚ A even though two values increase. In addition, the incensement of output torque (Torque_{avg}) can be shown when the MTPA control is applied during 0.2s ~ 0.3s compared to when $I_{de,ref}$ is 0 during 0.3s ~ 0.4s.

The simulation result of the FCS-MPC with DSVM under the speed variation of PMSG is shown in Fig. 18. $I_{s,ref}$ set as 10 A during the speed variation. Although the speed of PMSG increases, i_{qe} and i_{de} are controlled as $I_{de,ref}$ and $I_{qe,ref}$ beside the neutral-point voltage is maintained as almost zero which means that two dc-link voltages (V_{top}, V_{bottom}) have the same value.

Fig. 19 and 20 shows the key waveforms when the parameter is changed and the comparison results between the proposed FCS-MPC with DSVM and the conventional MPC [4] of Vienna rectifier at the same condition. In determining the control principle of the conventional MPC, the band of neutral-point voltage control is 2 V and weighting factor constant for reducing the number of the switching is zero to improve the current quality maximally. Although the control period of two methods is 200 us, the proposed method has the

This article has been accepted for publication in a future issue of this journal, but has not been fully edited. Content may change prior to final publication. Citation information: DOI 10.1109/TPEL.2019.2905843, IEEE Transactions on Power Electronics

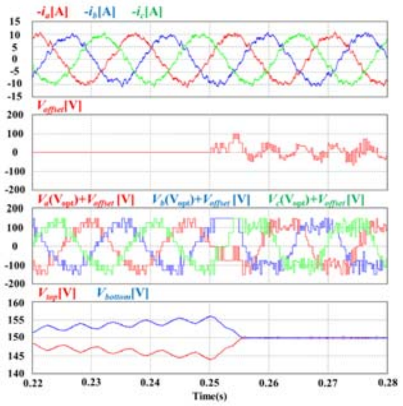

Fig. 16. Simulation results of the FCS-MPC with DSVM for identifying the neutral-point voltage control: 1200 r/m.

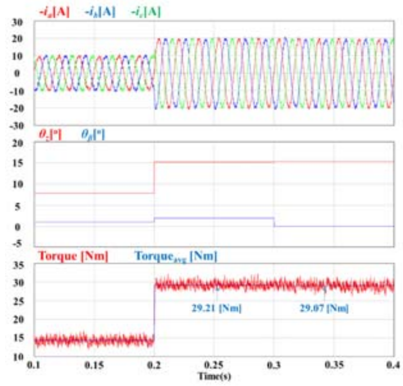

Fig. 17. Simulation results of the FCS-MPC with DSVM when $I_{s,ref}$ increases with and without MTPA : 1200 r/m.

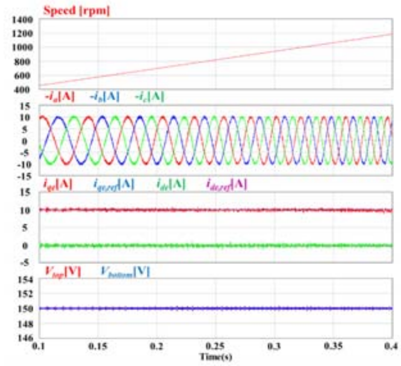

Fig. 18. Simulation results of the FCS-MPC with DSVM under the speed variation of PMSG.

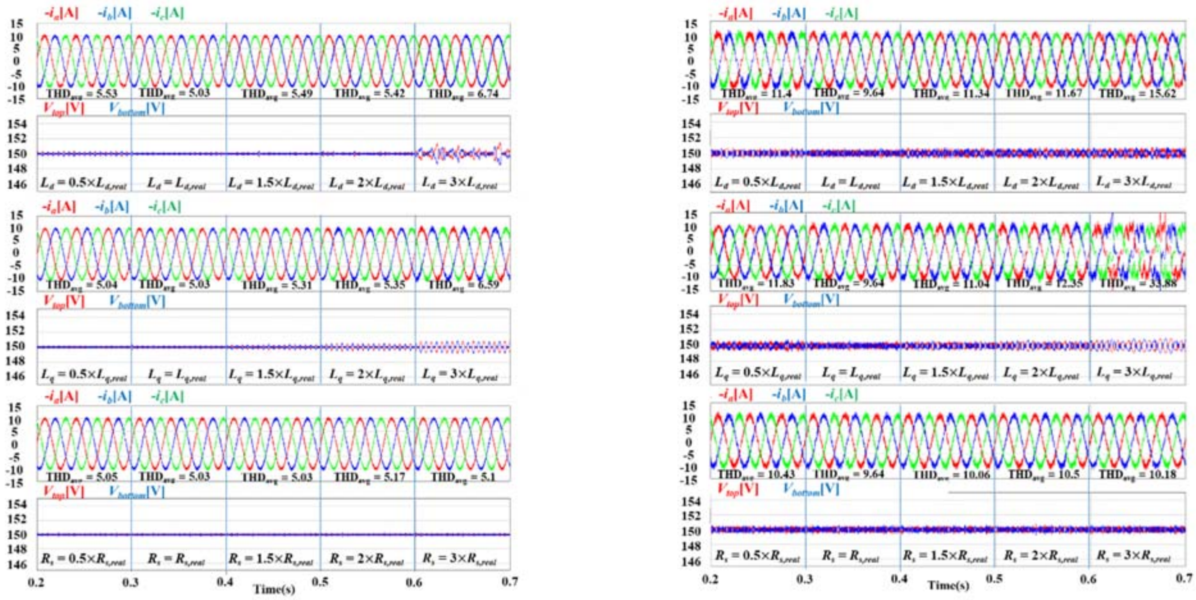

(a) (b)

Fig. 19. Comparison results for parameter (L_d, L_q and R_s) variation at $I_{s,ref}$ (10A) and speed (600 r/m). (a) The FCS-MPC with DSVM. (b) The conventional MPC [4].

lower total harmonic distortion (THD) of current than that of the conventional MPC in all results because the proposed method combines the MPC with the DSVM. Two methods show the similar tendency that the current quality and the neutral-point voltage ripple are aggravated as the L_d or L_q changes dramatically as shown in Fig. 19. In case of 3x$L_{d,real}$ and 3x$L_{q,real}$, however, the FCS-MPC with DSVM show the robustness more than the conventional MPC. On the other hand, the R_s variation does not influence on the performance of two methods. The one of reason is that the PMSG used in this paper has the small R_s to be negligible.

Although the FCS-MPC with DSVM has the robustness for L_d or L_q variation more than the conventional MPC, the large variation of λ_m is fatal for the FCS-MPC with DSVM as shown in Fig. 20. Since λ_m is the dominant factor for the $|V_{ref}|$ calculation in Step 1. Voltage vector selection, the large variation of λ_m leads to select the wrong voltage vectors of the undesired level in Table II and it make the current quality and neutral-point voltage ripple serious more than the conventional MPC.

VI. Experimental Results

The proposed FCS-MPC with DSVM for Vienna rectifiers was proved in experiment of three-level rectifier as shown in Fig. 21. The outer six switches of three-level rectifier are turn-off to operate as Vienna rectifier. The TMS320F28335 was used to control the experimental setup. The parameters in the simulation are used in the experiment

Fig. 22(a) and (b) show the comparison results between the proposed FCS-MPC with DSVM and the FCS-MPC with DSVM using all voltage vectors. The level showing $|V_{ref}|$ is 2 in Fig. 22(a) and the number of the candidate vector is twelve which is smaller than 19 (the number of all voltage vectors). Nevertheless, the effective voltage vector selection of the proposed FCS-MPC with DSVM guarantees the same current quality with the that of the FCS-MPC with DSVM using all

This article has been accepted for publication in a future issue of this journal, but has not been fully edited. Content may change prior to final publication. Citation information: DOI 10.1109/TPEL.2019.2905843, IEEE Transactions on Power Electronics

(a)

(b)

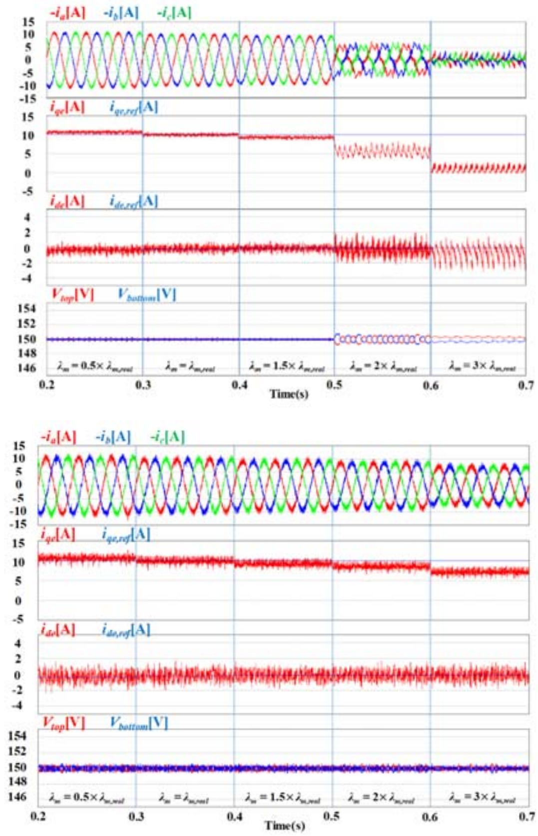

Fig. 20. Comparison results for parameter (λ_m) variation at $I_{s,ref}$ (10A) and speed (600 r/m). (a) The FCS-MPC with DSVM. (b) The conventional MPC [4].

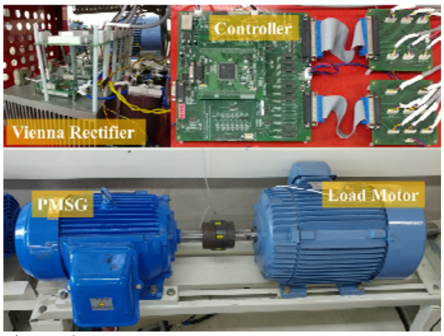

Fig. 21. Experimental setup.

(a)

(b)

(c)

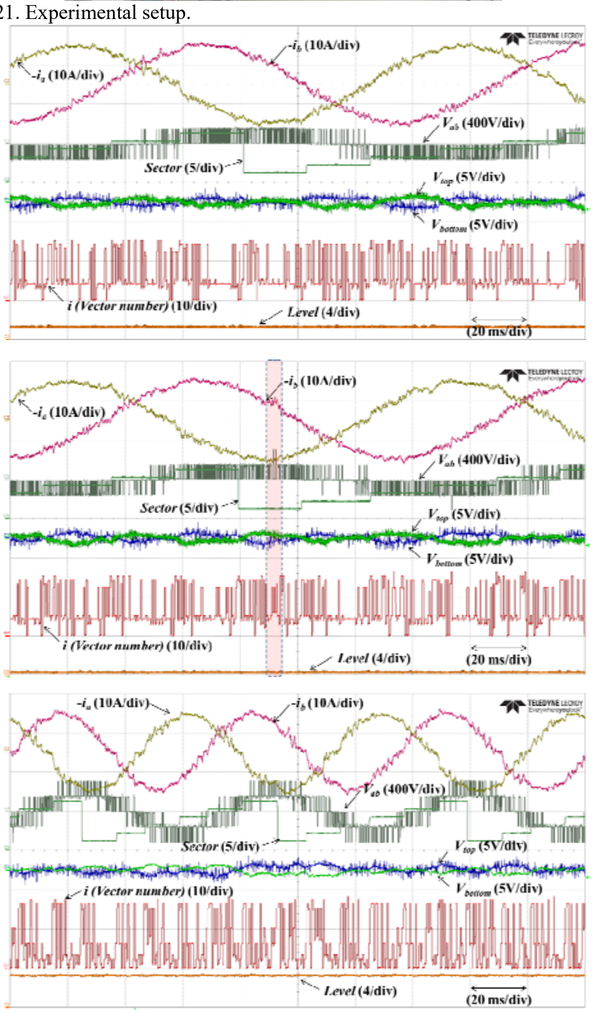

Fig. 22. Comparison results between the proposed FCS-MPC with DSVM and FCS-MPC with DSVM using all voltage vectors: $I_{s,ref}$ (10A). (a) The proposed FCS-MPC with DSVM (600r/m). (b) FCS-MPC with DSVM using all voltage vectors (600r/m). (c) The proposed FCS-MPC with DSVM (1200r/m).

vectors. In addition, the FCS-MPC with DSVM using all vectors aggravates rather the current quality as shown in dotted line of Fig. 22(b). It is because the current sampling noise makes the error in the optimal voltage selection. At high speed of Fig. 22(c), the proposed FCS-MPC with DSVM shows the same result of the simulation results.

The neutral-point voltage balancing results of the proposed FCS-MPC with DSVM are shown in Fig. 23. In both figures, V_{offset} is generated and it added to V_x(V_{opt}) to make the voltage difference between V_{top} and V_{bottom} zero. In addition, the waveforms of experimental results are the same as those of simulation results.

The calculation time of the proposed FCS-MPC with DSVM in TMS320F28335 was measured and compared to that of the FCS-MPC with DSVM using all voltage vectors. The results of the measurement depending on the level showing $|V_{ref}|$ are shown in Table V. In case of Level 0, the minimum time is shown because the minimum voltage vectors (four) are considered as the candidate vector. The level 3 has the maximum time owing to the largest number of candidate vectors. The proposed FCS-MPC with DSVM reduces the 26.8% of calculation burden averagely.

The proposed FCS-MPC with DSVM has the fast dynamic response as shown in Fig. 24. It is one of the characteristics that the FCS-MPC has. In addition, by increasing $I_{s,ref}$ the $\theta_z + \theta_\beta$ is changed from 4˚ to 8˚. it does not exceed 30˚ which is the operation limitation angle for Vienna Rectifier.

VII. Conclusion

In this paper, a finite control set-MPC (FCS-MPC) with the discrete space-vector modulation (DSVM) of Vienna rectifier for the permanent magnet synchronous generators (PMSGs) of wind turbine systems (WTSs) is proposed. The proposed FCS-MPC with DSVM effectively selects the candidate vectors for the cost function depending on the magnitude of the reference voltage calculated through the PMSG model, and it leads to the reduction of calculation burden. Furthermore, the

This article has been accepted for publication in a future issue of this journal, but has not been fully edited. Content may change prior to final publication. Citation information: DOI 10.1109/TPEL.2019.2905843, IEEE Transactions on Power Electronics

(a)

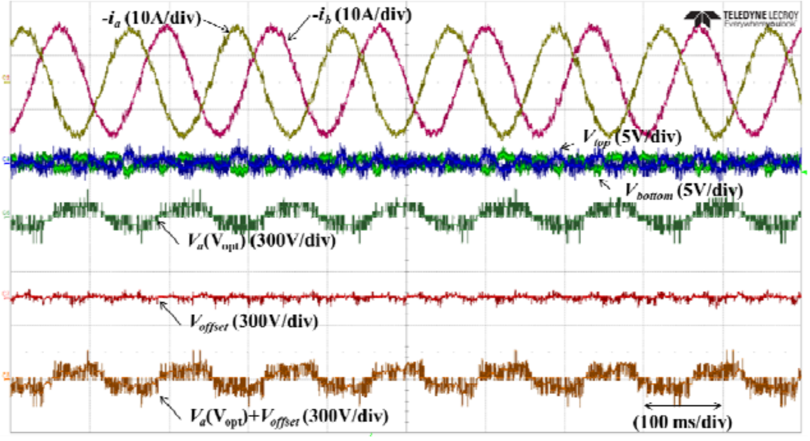

(b)

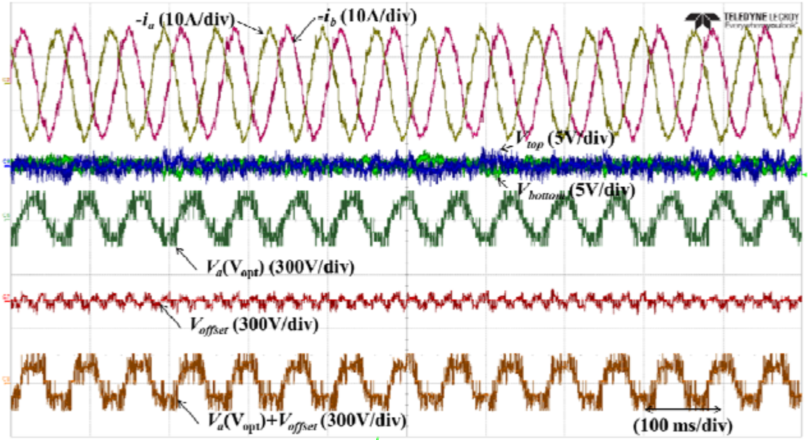

Fig. 23. Experimental results of the neutral-point voltage balancing of the proposed FCS-MPC with DSVM depending on the speed: $I_{s,ref}$ (10A). (a) Speed (600r/m). (b) Speed (1200r/m).

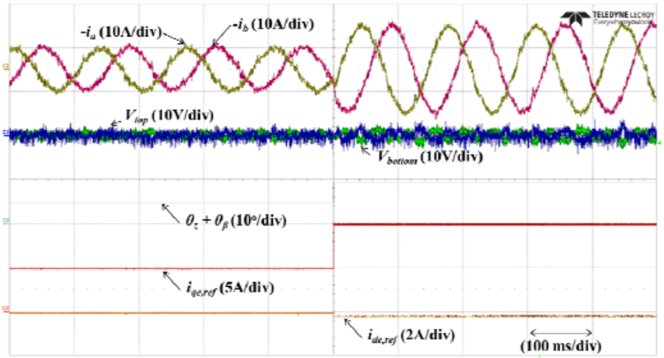

Fig. 24. Experimental results of the proposed FCS-MPC with DSVM when $I_{s,ref}$ increases 5A to 10A: 600 r/m.

DSVM causes that the current ripple component is mitigated and the neutral-point voltage is controlled as balance by the offset voltage calculated through the neutral-point voltage model of Vienna rectifier. Therefore, the proposed FCS-MPC with DSVM achieves the high performance of both the low current ripple and fast dynamic response. The performance and feasibility of the proposed FCS-MPC with DSVM are proved through the simulation and experimental results. In addition, the acceptable parameters of PMSG for applying the maximum torque per ampere (MTPA) control in Vienna rectifier are analyzed and it means that this paper suggests the guideline for using PSMG with Vienna rectifier. Since the assumption which is the speed and angle of PMSG do not changed during a control (sampling) period is considered in this paper, the control (sampling) period should be small enough than the time constant of PMSG speed to apply the proposed method.

TABLE V
COMPARISON RESULTS IN TERMS OF CALCULATION BURDEN

Level	The proposed FCS-MPC with DSVM	FCS-MPC with DSVM using all vectors
0	23.5 us (36% reduction)	
1	26 us (30% reduction)	
2	28 us (24% reduction)	37 us
3	30.5 us (18% reduction)	
4	27.5 us (26% reduction)	

REFERENCES

[1] J. W. Kolar and F. C. Zach, "A novel three-phase utility interface minimizing line current harmonics of high-power telecommunications rectifier modules," *IEEE Trans. Ind. Electron.*, vol. 44, no. 4, pp. 456–466, Aug. 1997.
[2] M. Leibl, J. W. Kolar, and J. Deuringer, "Sinusoidal Input Current Discontinuous Conduction Mode Control of the VIENNA Rectifier," *IEEE Trans. Power Electron.*, vol. 32, no. 11, pp. 8800–8812, Nev. 2017.
[3] J. Adhikari, P. IV, and S. K. Panda, "Reduction of Input Current Harmonic Distortions and Balancing of Output Voltages of the Vienna

Rectifier Under Supply Voltage Disturbances," *IEEE Trans. Power Electron*., vol. 32, no. 7, pp. 5802–5812, Jul. 2017.

[4] J. S. Lee and K. B. Lee, "Predictive Control of Vienna Rectifiers for PMSG Systems." *IEEE Trans. Ind. Electron*., vol. 64, no. 4, pp. 2580–2591, Apr. 2017.

[5] A. Rajaei, M. Mohamadian, and A. Y. Varjani, "Vienna-Rectifier-Based Direct Torque Control of PMSG for Wind Energy Application," *IEEE Trans. Ind. Electron*., vol. 60, no. 7, pp. 2919–2929, Jul. 2013.

[6] K. W. Hu and C. M. Liaw "Development of a Wind Interior Permanent-Magnet Synchronous Generator-Based Microgrid and Its Operation Control," *IEEE Trans. Power Electron*., vol. 30, no. 9, pp. 4973–4985, Sep. 2015.

[7] Thomas Nussbaumer; Johann W. Kolar, "Comparison of 3-Phase Wide Output Voltage Range PWM Rectifiers," *IEEE Trans. Ind. Electron*., vol. 54, no. 6, pp. 3422–3425, June. 2007.

[8] F. F. Bahamonde, H. V. Blavi, L. M. Salamero; J. M. Altés, and G. García, "Control of a three-phase AC/DC VIENNA converter based on the sliding mode loss-free resistor approach," *IET Power Electron*., vol. 7, no. 5, pp. 1073–1082, May 2014.

[9] R. Lai, F. Wang, R. Burgos, D. Boroyevich, D. Jiang, and D, Zhang, "Average Modeling and Control Design for VIENNA-Type Rectifiers Considering the DC-Link Voltage Balance," *IEEE Trans. Power Electron*., vol. 24, no. 11, pp. 2509–2522, Nov. 2009.

[10] J. S. Lee and K. B. Lee, "A Novel Carrier-Based PWM Method for Vienna Rectifier with a Variable Power Factor" *IEEE Trans. Power Electron*., vol. 63, no. 1, pp. 3-12, Jan. 2016.

[11] J. S. Lee and K. B. Lee, "Time-Offset Injection Method for Neutral-Point AC Ripple Voltage Reduction in a Three-Level Inverter," *IEEE Trans. Power Electron*., vol. 31, no. 3, pp. 1931-1941, Mar. 2016.

[12] L. Hang, B. Li, M. Zhang, Y. Wang, and L. M. Tolbert, "Equivalence of SVM and Carrier-Based PWM in Three-Phase/Wire/Level Vienna Rectifier and Capability of Unbalanced-Load Control," *IEEE Trans. Ind. Electron*., vol. 61, no. 1, pp. 20-28, Jan. 2014.

[13] X. Li, Y. Sun, H. Wang, M. Su, and S. Huang, "A Hybrid Control Scheme for Three-Phase Vienna Rectifiers," *IEEE Trans. Power Electron*., vol. 33, no. 1, pp. 629-640, Jan. 2018.

[14] R. Vargas, P. Cortes, U. Ammann, J. Rodrıguez, and J. Pontt, "Predictive control of a three-phase neutral-point-clamped inverter," *IEEE Trans. Ind. Electron*., vol. 54, no. 5, pp. 2697–2705, Oct. 2007.

[15] J. Scoltock, T. Geyer, and U. K. Madawala, "Model predictive direct power control for grid-connected NPC converters," *IEEE Trans. Ind. Electron*., vol. 62, no. 9, pp. 5319–5328, Sep. 2015.

[16] J. S. Lee, Y. Bak, K. B. Lee, and F. Blaabjerg, "MPC-SVM Method for Vienna Rectifier with PMSG used in Wind Turbine Systems," *in Proc. IEEE. App. Power Electron. Conf.*, pp. 3416-3421, 2016.

[17] Domenico Casadei, Member, IEEE, Giovanni Serra, Member, IEEE, and Angelo Tani, "Implementation of a Direct Torque Control Algorithm for Induction Motors Based on Discrete Space Vector Modulation," *IEEE Trans. Power Electron*., vol. 15, no. 4, pp. 769-777, Jul. 2000.

[18] Y. Wang et al., "Deadbeat Model-Predictive Torque Control with Discrete Space-Vector Modulation for PMSM Drives," *IEEE Trans. Ind. Electron*., vol. 64, no. 5, pp. 3537–3547, May 2017.

[19] S. Vazquez et al., "Model Predictive Control with Constant Switching Frequency using a Discrete Space Vector Modulation with Virtual State Vectors," *in Proc. IEEE Int. Conf. Ind. Technol*., Feb. 2009, pp. 1–6.

[20] J. Villegas, S. Vazquez, J. M. Carrasco, and I. Gil, "Model Predictive Control of a Switched Reluctance Machine using Discrete Space Vector Modulation," *in Proc. IEEE. Int. Symp. Ind. Electron*., Jul. 2010, 675 pp. 3137–3144.

[21] M. Preindl and S. Bolognani, "Model predictive direct speed control with finite control set of PMSM drive systems," *IEEE Trans. Power Electron*., vol. 28, no. 2, pp. 1007–1015, Feb. 2013.

[22] J. S. Lee and K. B. Lee, "Open-Switch Fault Tolerance Control for a Three-Level NPC/T-type Rectifier in Wind Turbine Systems," *IEEE Trans. Ind. Electron*., vol. 62, no. 2, pp. 1012-1021, Feb. 2015.

[23] N. Bedetti, S. Calligaro, C. Olsen, and R. Petrella, "Automatic MTPA Tracking in IPMSM Drives: Loop Dynamics, Design, and Auto-Tuning," *IEEE Trans. Ind. Appl*., vol. 53, no. 5, pp. 4547-4558, May 2017.

[24] T. Sun, J. Wang, and Xiao Chen, "Maximum Torque Per Ampere (MTPA) Control for Interior Permanent Magnet Synchronous Machine Drives Based on Virtual Signal Injection," *IEEE Trans. Power Electron*., vol. 30, no. 9, pp. 5036-5045, Sep. 2015.

June-Seok Lee (S'11-M'15) received the B.S., M.S., and Ph.D. degrees in electrical and computer engineering from Ajou University, Suwon, Korea, in 2011, 2013, and 2015, respectively. Since 2015, he has been with the Korea Railroad Research Institute, Uiwang, Korea.

His research interests include high power electric machine drives, grid-connected systems, multilevel inverters and reliability.

Kyo-Beum Lee (S'02–M'04–SM'10) received the B.S. and M.S. degrees in electrical and electronic engineering from the Ajou University, Suwon, South Korea, in 1997 and 1999, respectively. He received the Ph.D. degree in electrical engineering from the Korea University, Seoul, South Korea, in 2003. From 2003 to 2006, he was with the Institute of Energy Technology, Aalborg University, Aalborg, Denmark. From 2006 to 2007, he was with the Division of Electronics and Information Engineering, Chonbuk National University, Jeonju, South Korea. In 2007, he joined the Department of Electrical and Computer Engineering, Ajou University.

His research interests include electric machine drives, renewable power generation, and electric vehicle applications.

Dr. Lee is an Associated Editor of the IEEE Transactions on Power Electronics, the Journal of Power Electronics, and the Journal of Electrical Engineering and Technology.

Frede Blaabjerg (S'86-M'88-SM'97-F'03) received the Ph.D. degree in electrical engineering from Aalborg University, Aalborg, Denmark, in 1992.

He was with ABB-Scandia, Randers, from 1987-1988. He became an Assistant Professor in 1992, an Associate Professor in 1996 and a full professor in power electronics and drives in 1998. From 2017, he became a Villum Investigator. His current research interests include power electronics and its applications such as in wind turbines, PV systems, reliability, harmonics and adjustable speed drives. He has published more than 500 journal papers in the fields of power electronics and its applications. He is the co-author of two monographs and editor of 7 books in power electronics and its applications.

Dr. Blaabjerg received 24 IEEE Prize Paper Awards, the IEEE PELS Distinguished Service Award in 2009, the EPE-PEMC Council Award in 2010, the IEEE William E. Newell Power Electronics Award 2014 and the Villum Kann Rasmussen Research Award 2014. He was the Editor-in-Chief of the IEEE TRANSACTIONS ON POWER ELECTRONICS from 2006 to 2012. He has been Distinguished Lecturer for the IEEE Power Electronics Society from 2005 to 2007 and for the IEEE Industry Applications Society from 2010 to 2011 as well as 2017 to 2018. In 2018, he is President Elect of IEEE Power Electronics Society.

He is nominated in 2014, 2015, 2016 and 2017 by Thomson Reuters to be between the most 250 cited researchers in Engineering in the world. In 2017 he became Honoris Causa at University Politehnica Timisoara (UPT), Romania.